AJNR Am J Neuroradiol 20:63–73, January 1999

Dynamic CT Measurement of Cerebral Blood Flow: A Validation Study

Aleksa Cenic, Darius G. Nabavi, Rosemary A. Craen, Adrian W. Gelb, and Ting-Yim Lee

BACKGROUND AND PURPOSE: **Our objective was to develop a method to correct for the effect of partial volume averaging (PVA) in the CT measurement of contrast enhancement in small arteries, and to validate a dynamic contrast-enhanced CT method for the measurement of regional cerebral blood flow (rCBF).**

METHODS: **Contrast-enhanced CT scans of tubes of known inner diameters were obtained to estimate the size-dependent scaling factors (PVSF) due to PVA. The background-subtracted image profiles of the contrast-filled tubes were fitted to gaussian curves, and the standard deviations (SDs) of these curves were correlated with the PVSF of each tube. In the second part of this investigation, 13 studies were performed in six New Zealand white rabbits under normal conditions. Dynamic CT measurements of rCBF, regional cerebral blood volume (rCBV), and regional mean transit time (rMTT) were calculated in the left and right parietal lobes and the basal ganglia. The CT rCBF values were compared with those obtained by the microsphere method, which is the standard of reference.**

RESULTS: **We found strong correlations for the SDs of the gaussian curves to the known inner diameters of the tubes and to their size-related PVSF. These correlations demonstrated that the error from PVA in the measurement of arterial enhancement can be corrected without knowledge of the actual size of the artery. The animal studies revealed a mean (±SD) rCBF of 73.3 ± 31.5 mL/100 g per minute, a mean rCBV of 1.93 ± 0.74 mL/100 g, and a mean rMTT of 1.81 ± 1.02 seconds. A strong correlation was found between rCBF values derived by the CT and the microsphere methods.**

CONCLUSION: **We have validated a new dynamic CT method for measuring rCBF. The accuracy of this technique suggests that it can be used as an alternative diagnostic tool to assess the cerebral hemodynamics in experimental and clinical situations.**

Cerebrovascular disorders such as ischemic and hemorrhagic strokes constitute the third most frequent cause of death and disability in North America (1). Despite considerable progress in stroke treatment, cerebrovascular disorders remain a frequent challenge in acute neurovascular management (2). Moreover, since new therapeutic options, such as thrombolytic therapy, are expensive and are accompanied by potentially life-threatening complications (2), assessment of the risk-benefit ratio on an individual basis is crucial for prognostic and socioeconomic reasons (3). Above all, the location and extent of the ischemic lesion, together with the severity of the blood flow reduction, are the main factors that predict outcome in the treatment of stroke (4). Thus, a significant clinical demand exists to assess cerebral hemodynamics in order to guide the decision between a conservative or a more aggressive form of therapy in the early stage of stroke.

Several methods have been used to investigate cerebral hemodynamics in acute cerebrovascular disease (5). Positron emission tomography (PET) is the current standard of reference for the in vivo assessment of regional cerebral blood flow (rCBF), blood volume (rCBV), and brain metabolism (6). However, owing to the high operational costs and

Received June 25, 1998; accepted after revision September 28.

Supported by the Medical Research Council of Canada and the Academic Development Fund of the London X-ray Associates, London, Ontario. D.G.N., on leave from the Department of Neurology, University of Muenster, Germany, was supported by a research grant from the Deutsche Forschungsgemeinschaft.

Presented in part at the annual meeting of the American Society of Neuroradiology, Toronto, Canada, May 1997.

From the Imaging Research Laboratories, John P. Robarts Research Institute (A.C., D.G.N., T-Y.L.); the Medical Biophysics Department, The University of Western Ontario (A.C., T-Y.L.); the Lawson Research Institute, St Joseph's Health Centre, (A.C., T-Y.L.); and the Department of Anaesthesia, University Campus, London Health Sciences Centre (R.A.C., A.W.G.), London, Ontario, Canada.

Address reprint requests to Ting-Yim Lee, PhD, Imaging Research Laboratories, John P. Robarts Research Institute, P.O. Box 5015, 100 Perth Dr, London, Ontario, N6A 5K8, Canada.

low clinical availability, its application in stroke is restricted to specific scientific investigations and is not suitable for routine clinical use. Single-photon emission CT (SPECT) has been suggested as a tool to stratify stroke patients according to type and severity of disease (7). However, the low spatial resolution and the inability to calculate absolute blood flow values represent major drawbacks of SPECT. MR imaging with diffusion and perfusion weighting is an intriguing new method to assess tissue viability (8–10). Nevertheless, the relatively high costs and limited clinical availability of MR imaging for patients suffering acute stroke warrant a search for alternative diagnostic techniques.

Since a CT scan of the brain is the first diagnostic imaging study obtained in patients with acute stroke, various attempts have been made during the last two decades to establish a CT-based method to calculate rCBF and rCBV (11–16). The widespread availability of CT scanners, together with their high image quality and low costs, are attractive features of this approach. Moreover, by simply extending the routine CT examination, this method would prevent time-consuming transport of patients between scanners, further delaying treatment.

Besides the xenon-based method (17), the published CT techniques rely on an intravenous bolus injection of a radiologic contrast material and rapid serial (dynamic) CT scanning to detect the blood flow–related changes in brain tissue enhancement or the increase in CT number (18). However, most of these techniques can only provide relative blood flow and blood volume values by side-to-side comparisons of the changes in contrast enhancement with respect to time (12, 13). This assumes that the contralateral side is normal; however, stroke patients rarely have unilateral disease. In the case of bilateral disease, the choice of the reference ''normal'' region becomes problematic.

The critical problem in the measurement of absolute rCBF values with contrast-enhanced dynamic CT scanning is the calculation of the regional mean transit time (rMTT) through the brain (19, 20). The latter calculation requires the simultaneous measurement of the tissue and the intraarterial contrast enhancement curves as functions of time after a bolus injection of contrast material (21). Deconvolution between these two curves gives the MTT in the brain. Owing to the limited scanning frequency of the CT scanners in the past (only one CT scan every few seconds) and the problem of partial volume averaging (PVA) while scanning small arteries, this method of calculating MTT was of low accuracy (21). Besides deconvolution, several alternative approaches have been proposed to evaluate the global and regional MTT based on CT scanning, some with promising experimental and clinical results (14, 15, 22). However, as compared with the more rigorous deconvolution method, these approaches require a number of assumptions that may not be correct in the general case. Further, PVA correction of the imaged cerebral arteries was generally not considered. Using venous blood samples from dynamic CT studies, Lapin et al (23) showed that PVA may decrease the CT number in a given voxel within a cerebral artery by as much as four times. This study showed the importance of correcting for PVA when imaging small arteries to obtain accurate arterial contrast enhancement for CT rCBF studies.

By using a slip-ring third-generation CT scanner to scan at the rate of one scan per second, we developed a dynamic CT technique to calculate the rMTT and to measure absolute rCBF and rCBV. The objectives of this experimental study were to develop a new method to correct for PVA, allowing accurate measurement of intraarterial contrast enhancement curves, and to investigate the accuracy of our CT-derived rCBF values in an animal model by comparing them with measurements obtained by the microsphere method.

Theory

The theoretical basis of our CT CBF measurement technique is the central volume principle, first discussed by Meier and Zieler (24), and later extended by Roberts and Larson (25).

Central Volume Principle

Consider a network of capillaries in the brain. The rate of CBF into this network is CBF mL/min per gram, and the CBV in it is CBV mL/g. Owing to the different possible path lengths that can be followed, blood elements flowing through the network will require different lengths of time (ie, transit times) to travel from the arterial input to the venous outlet. The average of all possible transit times through this capillary network is the MTT. The central volume principle relates CBF, CBV, and MTT in the following simple relationship:

$$\text{CBF} = \frac{\text{CBV}}{\text{MTT}} \quad (1)$$

In order to apply the central volume principle, we have to make blood flow detectable by the CT scanner. This is achieved by injecting contrast material into the bloodstream. We also assume that a linear relationship exists between the enhancement in CT numbers and the concentration of contrast material within an artery or brain tissue region, and that contrast material and blood have the same hemodynamic properties. To describe the response of the CT scanner to contrast material, we also need to introduce two important concepts, the impulse residue and the tissue residue functions.

Impulse and Tissue Residue Functions

If radiologic contrast material is injected at the arterial input as a bolus of very short duration (ie,

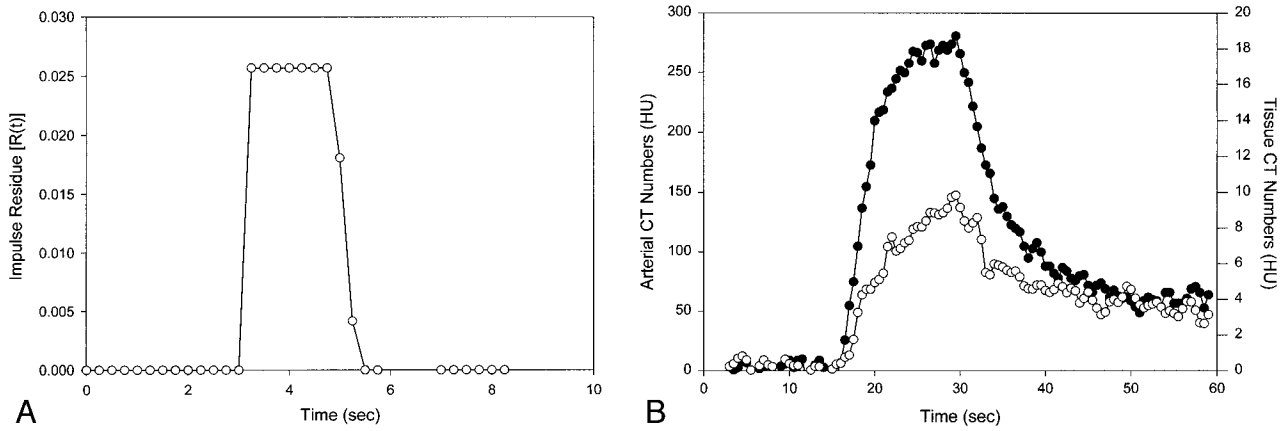

FIG 1. *A,* Example of the impulse residue function of the brain, R(t), obtained by deconvolution of $C_a(t)$ and Q(t) in *B,* illustrating the expected general shape.

B, Examples of arterial, $C_a(t)$ (*closed circles*), and regional brain tissue, Q(t) (*open circles*), contrast-enhancement curves obtained from dynamic CT scanning.

impulse injection) and the mass of contrast agent that remains in the capillary network over time is measured with a CT scanner, an enhancement curve of the shape shown in Figure 1A will be observed. This is called the impulse residue function, R(t) (26).

The distinguishing features of R(t) are an initial flat plateau followed by a continuous decrease toward the zero baseline (Fig 1A). The duration of the plateau corresponds to the time interval during which all the injected contrast material remains in the capillary network. Following this time interval, contrast material begins to leave the network, leading to the observed drop in R(t). The significance of the impulse residue function is that it is used to calculate the MTT according to the area over height formula (21):

$$2) \qquad \text{MTT} = \frac{\text{area underneath R(t)}}{\text{height of R(t) plateau}}$$

The direct experimental determination of R(t) is not possible because it is difficult to identify the specific arterial inlet(s) of a brain region. Even if it were possible, the procedure is highly invasive and would render the method inapplicable to patients. Instead, contrast material is intravenously injected at a peripheral vein and the mass of the injected material that resides in the capillary network is measured with a CT scanner. The measured function in this case is called the tissue residue function, Q(t). If blood flow is constant and the enhancement at the arterial input is linear with respect to contrast concentration, then Meier and Zieler (24) showed that

$$3) \qquad Q(t) = \text{CBF} \times [C_a(t)^* R(t)]$$

where $C_a(t)$ is the enhancement curve measured at the arterial input, and * denotes the *convolution* operator. In essence, the convolution operation involves the addition of many copies of the same R(t) except for the fact that each copy is multiplied by the arterial contrast enhancement at a different time and then shifted in time by a different amount. In our application of Equation 3, we also assume that $C_a(t)$ can be measured at a peripheral artery, such as the ear artery.

Deconvolution

As discussed above, if R(t) and $C_a(t)$ are known, Q(t) can be calculated by their convolution. However, owing to the experimental limitations discussed above, R(t) is difficult, if not impossible, to measure. Instead, Q(t) and $C_a(t)$ are measured with the CT scanner (Fig 1B). The process of calculating R(t), given Q(t) and $C_a(t)$, is the opposite (inverse) of convolution and is called *deconvolution.* It is known that the deconvolution process is extremely sensitive to noise in the measured arterial and tissue-enhancement curves (19, 20). Without reliable methods to limit the deleterious effects of noise, the calculated R(t) will be wildly oscillatory, making the calculation of MTT, according to Equation 2, impossible.

We reduced the noise sensitivity of deconvolution by using an algorithm previously (27) developed so that solutions of the general shape shown in Figure 1A are always produced.

Cerebral Blood Volume Calculation

As discussed by Axel (18), the volume of flowing blood (ie, CBV) in a capillary network can be calculated by the ratio of areas:

$$4) \qquad \text{CBV} = \frac{\text{area underneath Q(t)}}{\text{area underneath Ca(t)}}$$

where Q(t) and $C_a(t)$ are the tissue and arterial enhancement curves, respectively. A typical set of Q(t) and $C_a(t)$ is shown in Figure 1B. As stated by Axel (18), this method is only feasible when the

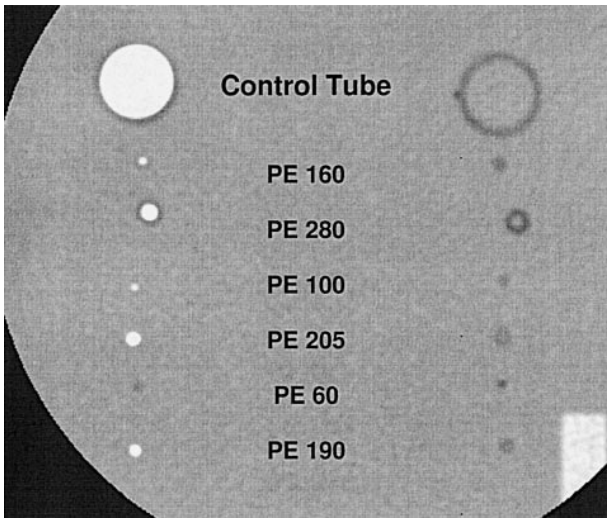

FIG 2. Axial CT scan of the PE tubes phantom used to correct for PVA. PE tubes on the left contain 40 mL of distilled water with 2.7 mL of Isovue 300 (300 mg I/mL contrast material) added. PE tubes on the right contain only distilled water to serve as background (ie, unenhanced). A two-pixel-radius ROI was drawn in the center of each tube, and the mean CT number was determined within these circular ROIs.

blood-brain barrier is intact (eg, normal cerebral tissue) and there is no recirculation of contrast material. In cases in which the blood-brain barrier is compromised (eg, tumor, infarction, abscess), Q(t) would be a summation of the enhancement due to contrast material in both the intravascular and extravascular spaces, and CBV would be overestimated. To eliminate the effect of recirculation from both $C_a(t)$ and Q(t), we adopted the following procedure: the trailing slope of $C_a(t)$ was extrapolated with a monoexponential function. The extrapolated $C_a(t)$ was then convoluted with the calculated R(t) to generate the recirculation-corrected Q(t). CBV was calculated as the ratio of the area underneath the recirculation-corrected Q(t) to that of the recirculation-corrected $C_a(t)$.

Methods

CT Partial Volume Averaging Correction

A partial volume phantom was constructed to determine the effect of PVA when imaging small arteries. Figure 2 shows a CT scan of a cross section of this phantom. The phantom consisted of one pair of 10-mm-diameter tubes (the control tubes) and six pairs of smaller polyethylene (PE) tubes, varying in diameter from 0.76 mm to 2.15 mm (PE-60 to PE-280). For each pair of tubes, the background tube was filled with distilled water while the contrast tube was filled with a contrast solution (20 mg I/mL) made from the same batch of distilled water. The 10-mm-diameter control tubes were large enough so that PVA was negligible. In order to acquire precise CT number measurements, the phantom was scanned 10 times at the same cross section using the same scanning parameters as in the rabbit studies described below. From the averaged image of these 10 scans, the mean CT number within each tube was obtained by drawing a two-pixel-radius region of interest (ROI) in the center of each tube. The mean CT number in each background tube was then subtracted from the mean CT number in the same-size contrast tube to give the enhancement, M, due to the contrast solution for that particular diameter. The partial volume scaling factor (PVSF) for each size of PE tube was determined as follows:

$$\text{PVSF} = \frac{\text{M(control tube)}}{\text{M(PE tube)}} \quad (5)$$

Since the inner diameters of the PE tubes were known, each tube diameter could be correlated to the calculated PVSF value. From this correlative relationship, the PVSF for any other tube diameter can be found.

When imaging an artery with a CT scanner, one does not have prior knowledge of the artery's diameter; hence, the corresponding PVSF to be used is not known. We developed the following method to provide an estimate of the diameter of an artery. Image profiles (mean CT number plotted against image pixels) of the artery were obtained from a noncontrast image and from a contrast-enhanced image (when the mean CT number was at its maximum in the vessel ROI). The noncontrast image profile was subtracted from the enhanced profile to give the background-subtracted image profile. To improve the accuracy in the subsequent determination of its width, the background-subtracted profile was interpolated to one fifth of a pixel. A gaussian curve was then fitted to this interpolated, background-subtracted image profile of the artery. The standard deviation (SD) of the gaussian curve then served as a measure of the imaged artery's diameter. The image profiles of the PE tubes in the phantom were similarly subtracted and fitted with gaussian curves. A calibration curve was then generated by correlating the SD value for each PE tube with its associated PVSF value. From the calibration curve, the PVSF for the artery was determined, knowing the SD of the gaussian fit to its background-subtracted image profile. The true $C_a(t)$, corrected for PVA, was the experimentally measured $C_a(t)$ scaled by this PVSF.

Animal Protocol

Six healthy male New Zealand white rabbits were used in experiments approved by the animal ethics committee at the University of Western Ontario. Each rabbit was surgically prepared by inducing anesthesia via a mask with halothane, and one ear vein was cannulated for administration of a muscle relaxant (vecuronium bromide) during the experiment. After a tracheotomy was performed, the rabbits were mechanically ventilated to a normocapnic $PaCO_2$ of 40 $\pm$ 3 mm Hg with a mixture of air and oxygen (FiO_2 0.4). Both femoral arteries were catheterized to allow arterial blood sampling for hematocrit and blood gas determination and measurement of mean arterial pressure (MAP). Both femoral veins were also catheterized for fluid and drug administration if required (eg, phenylephrine for maintenance of MAP between 75 and 85 mm Hg). Isoflurane anesthesia was then induced at 1 MAC (minimum alveolar concentration). Finally, a thoracotomy was performed with the insertion of a catheter into the left atrial appendage for the injection of fluorescent microspheres required in the ex-vivo measurement of rCBF. Local anesthetic (lidocaine 1.0%) was administered for all surgical wounds.

With the surgical procedures completed, the rabbit was placed prone on the patient's couch of the CT scanner with its head secured in a head holder. In order to have an ear artery in the same scan plane as the brain, a specially designed holder was used to fix the ear horizontally over the rabbit's head (Fig 3).

MAP was continuously monitored and rectal temperature was maintained at 38.5°C with a heated, recirculating water pad and a heat lamp. Hematocrit was measured every 30 minutes.

CT Protocol

The imaging studies were obtained with a slip-ring CT scanner, which results in the continuous acquisition of images (ie,

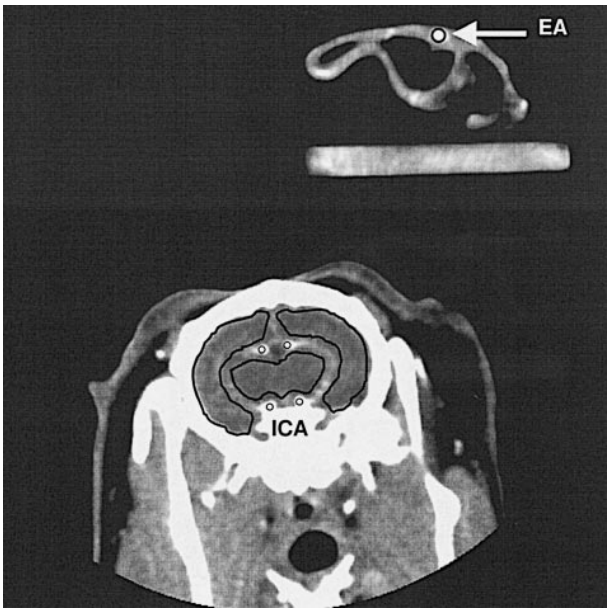

FIG 3. Contrast-enhanced coronal CT scan of a rabbit. Two parietal ROIs of similar size and one central region in the basal ganglia, as shown on the image, were used for all measurements of rCBF. An ear artery (EA) was used to measure the arterial enhancement curve. The postcommunicating arteries (in the middle of the brain) and the internal carotid arteries (ICA) are also visible.

cine scanning) from the 360° per second unidirectional rotation of the X-ray tube and detector assembly about the gantry. In our scanning protocol, for a total study time of 60 seconds, 60 rotations were made as the CT couch remained stationary. We have shown that the first cerebral circulation time of intravenously injected contrast material in rabbits is less then 60 seconds (Fig 1B); hence, the chosen scan time was sufficient to provide an accurate representation of the arterial and tissue hemodynamics.

The CT protocol involved two steps: the coronal localization scans and the dynamic (cine) CT scans. For localization, unenhanced coronal scans were obtained at 1-mm intervals with parameters of 120 kVp, 80 mAs, 512 × 512 matrix, 10-cm field of view, and 3-mm section thickness. From these coronal scans, the image containing the optic chiasm was chosen as the study section. The optic chiasm served as a marker to register microsphere rCBF measurements with CT rCBF measurements. Finally, with the level of the optic chiasm localized, a dynamic CT study was performed with parameters of 80 kVp, 80 mAs, 512 × 512 matrix, 10-cm field of view, and 3-mm section thickness. The back-projection filter used in the reconstruction of CT scans had a cut-off frequency of 10 lp/cm. CT scanning was initiated 5 seconds before contrast material (Isovue 300, 1.5 mL/kg body weight) was intravenously injected via the cannulated ear vein using an automatic injector (Medrad Injector, Medrad, PA) at the rate of 0.3 mL/s. This delay in contrast material injection allowed for the acquisition of unenhanced baseline images. Dynamic CT scanning was maintained during the bolus injection of contrast material and continued for a total of 60 seconds.

From the raw CT projection data, it was possible to retrospectively reconstruct the 1-second images at arbitrary time intervals. In our studies, to improve time resolution, the time interval between sequential images was set at 0.5 seconds. This procedure has a low-pass filtering effect on the tissue and arterial enhancement curves obtained from the reconstructed images. The reduced noise level in the enhancement curves would improve the stability of the subsequent deconvolution process. We have established that the noise correlation introduced by this filtering of the enhancement curves does not significantly affect the calculation of the impulse residue function by our deconvolution algorithm.

Regional CBF Measurements Using Fluorescent Microspheres

To validate our CT rCBF measurements, rCBF was also measured using fluorescent microspheres (Interactive Medical Technologies, Los Angeles, CA) as the standard of reference. This ex-vivo technique has been used for the past 20 years for validating other rCBF measurement methods (28). In our study protocol, rCBF was first measured by using the microsphere technique, and then immediately afterward by the dynamic CT technique. The close spacing in time (time delay < 1 minute) ensured that similar hemodynamic conditions existed during both measurement techniques. In addition, arterial blood gases were determined immediately before and after each rCBF measurement technique to verify that similar $PaCO_2$ levels existed throughout the two measurements. For each microsphere study, fluorescent microspheres (15-μ diameter) of a particular color were randomly selected from a group of six possible colors and injected (1.5 million spheres) into the left atrium. Using a syringe pump, 3.0 mL of blood was withdrawn from a femoral artery at a rate of 1.0 mL/min for 3 minutes, starting 1 minute before microsphere injection. Upon completion of the experiment, the brain was removed, sectioned into 5-mm-thick sections, and the section through the optic chiasm was trimmed to obtain three regions corresponding to the same ROIs as on the CT scans. Regional tissue CBF was then calculated for each tissue sample using the equation

$$6) \qquad CBF_t = \frac{N_t \times Q}{R}$$

where CBF_t is the rCBF of the brain tissue sample in mL/100 g per minute, N_t is the number of microspheres detected in the tissue sample normalized to 100 g, Q is the rate of aspiration (1.0 mL/min), and R is the total number of microspheres detected in the volume of blood extracted.

Repeated Studies

In five of the six rabbits, two or three sequential studies were performed. In one rabbit, only one study was completed owing to its sudden death. The sequential studies were separated by at least 30 minutes to allow the contrast material from the previous injections to wash out of the circulatory system.

CT Data Analysis

The CT data were stored on digital audiotape and then transferred to a Sun Ultra I (Sun Microsystems; Mountain View, CA) workstation for further computational analysis.

For the determination of the tissue residue curve, Q(t), three ROIs in the brain (two in the parietal regions and one in the basal ganglia), as shown in Figure 3, were used. These tissue ROIs were drawn such that no major blood vessels were present within them. For those animals that had repeated studies, identical ROIs were used in each of the studies to maintain similar tissue composition and pixel areas in the regions used. Q(t) for each region was obtained by subtracting the regional mean baseline CT number on noncontrast scans from the mean CT number on sequential contrast-enhanced scans.

The arterial contrast-enhancement curve, $C_a(t)$, was determined with a two-pixel-radius circular ROI in an artery. As shown in Figure 3, several arteries were present in the plane of the CT scan. The artery used for determining $C_a(t)$ was the one with the largest diameter on the CT scan and yielded the highest mean CT number at peak contrast enhancement. This procedure was followed to minimize PVA effects in $C_a(t)$. In

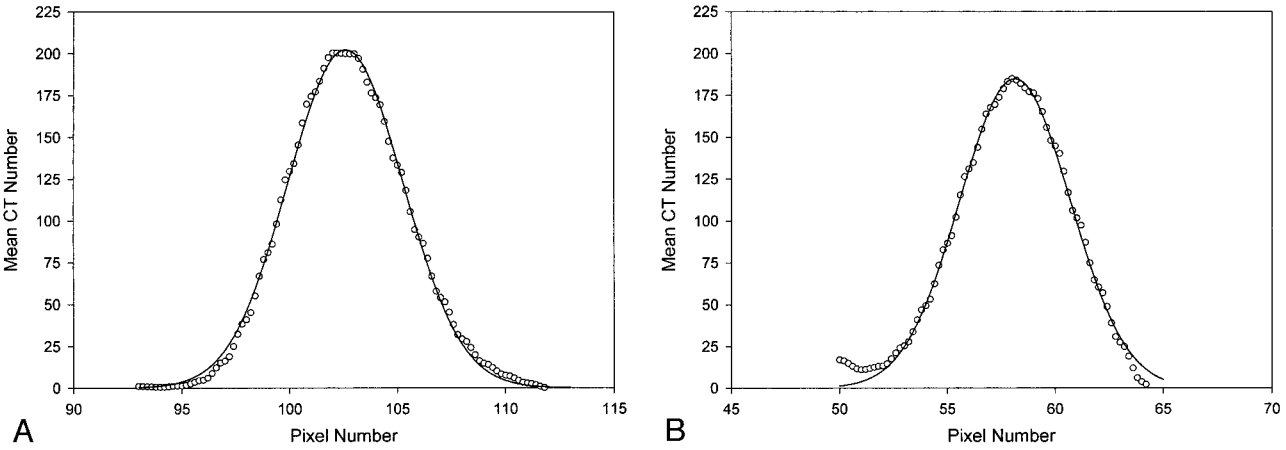

FIG 4. *A,* Background-subtracted image profile of a PE-160 tube with the fitted gaussian curve. The calculated gaussian SD was 2.58 for the known inner diameter of 1.14 mm.

B, Background-subtracted image profile of a rabbit ear artery with the fitted gaussian curve. The calculated gaussian SD was 2.58, corresponding to an estimated inner diameter of about 1.14 mm for the ear artery.

most rabbit studies, the ear artery was used. However, in cases in which the ear artery was not sufficiently distinct (eg, when phenylephrine was used to maintain the MAP), one of the cerebral arteries was selected to obtain $C_a(t)$. As in the measurement of Q(t), $C_a(t)$ was also determined by subtracting the mean baseline CT number in the vessel ROI on noncontrast scans from the mean CT number on contrast-enhanced scans. The background-subtracted image profile of the artery was then obtained and fitted with a gaussian curve. From the SD of the gaussian curve, the PVSF of the artery was found and the measured $C_a(t)$ was scaled by this factor to correct for PVA.

Statistics

Statistical analysis was performed using the Jandel Scientific Software Package (Sigma Plot and Sigma Stat). Standard descriptive statistics parameters, such as mean ± SD values, were found. A *t*-test and Mann-Whitney rank sum test were used to compare normally and abnormally distributed data, respectively. One-way ANOVA for repeated measurements was used to determine the variability of the cerebral hemodynamic measurements. Nonlinear regression was used to determine the calibration relationship between PVSF and SD of gaussian fits of the background-subtracted image profiles of PE tubes in the partial volume phantom. Linear regression analysis was used to compare the rCBF values derived by the CT and the microsphere techniques. Pearson product moment correlation was used to provide linear correlation coefficients. Statistical significance was declared at the $P < .05$ level.

Results

CT Partial Volume Averaging Correction

From a series of CT scans of the partial volume phantom (Fig 2), background-subtracted image profiles were generated for the cross sections of the individual tubes. Figure 4A shows a typical profile through the center of a given tube of the phantom. Moreover, the gaussian curve provides an excellent fit for this CT-measured profile. A significant linear correlation was found between the inner diameters and the gaussian SDs of the imaged PE tubes ($r = 0.998$, $P < .001$). This linear relationship was represented by the following regression equation (Fig 5A):

$$7) \qquad SD = 1.38 + 1.05 \times ID$$

where SD is the number of pixels, and ID is the inner diameter of a PE tube (in mm). This linear relationship confirms the assumption that the gaussian SD is a reliable measure of the inner diameter of a PE tube imaged in cross section.

In plotting PVSFs against the gaussian SDs for the PE tubes in the partial volume phantom (Fig 5B), we found a significant exponential relationship between the two parameters ($r = 0.996$, $P < .001$). From this exponential fit, we derived the following mathematical relationship between the gaussian SD of a PE tube and its PVSF:

$$8) \qquad PVSF = 1.0 + 2576\exp(-3.17 \times SD)$$

For an imaged artery of unknown inner diameter, its gaussian SD could be easily obtained by fitting its background-subtracted image profile (Fig 4B), as discussed in the Methods section, and the PVSF determined from Equation 8. In the rabbit studies, the SDs were found to range from 2.4 to 2.8, and the corresponding PVSFs from Equation 8 were between 2.3 to 1.4.

Regional CBF and CBV Measurements in Rabbits

Details of the monitored physiological parameters for the six rabbits are listed in Table 1. Using a paired *t*-test, no statistically significant change ($P >$. 1) was found in the physiological parameters over the duration of the repeated studies. However, owing to the withdrawal of intravenous and arterial blood samples over time, a slight decrease in hematocrit was observed (Table 1).

The mean regional values (±SD) of the measured hemodynamic parameters for both the dy-

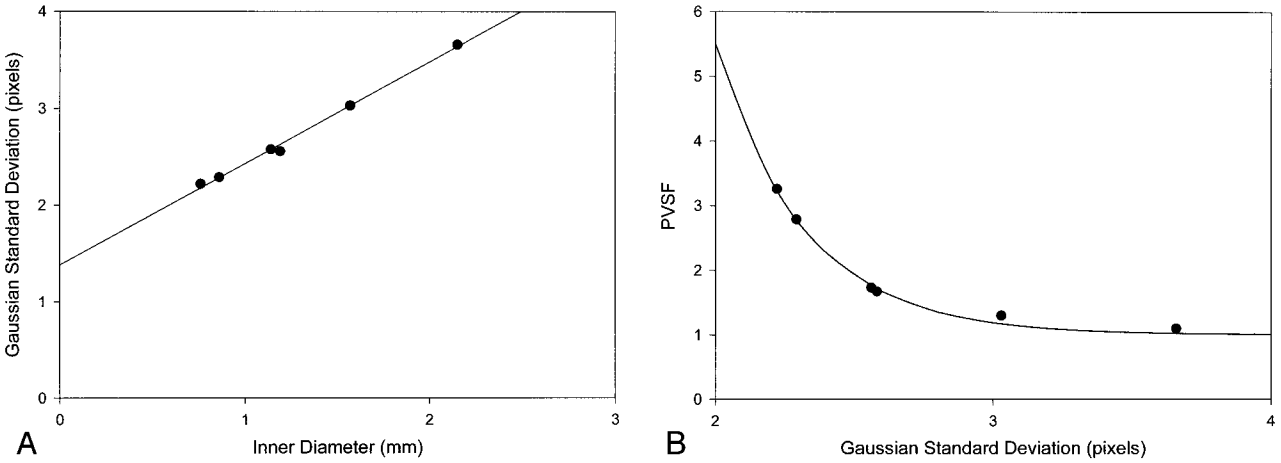

FIG 5. Results of the PE tubes phantom experiments.
A, A significant linear correlation was found between the gaussian SDs and the inner diameters of the PE tubes ($r = .998$, $P < .001$).
B, PVSF calibration curve obtained from the PE tubes phantom (Fig 2). A significant exponential correlation was found between PVSF and gaussian SDs for the PE tubes ($r = .996$, $P < .001$).

TABLE 1: Monitored physiological and measured cerebral hemodynamic parameters

	Study 1 (n = 18)	Study 2 (n = 15)	Study 3 (n = 6)	Total (n = 39)
Physiological parameters				
$PaCO_2$ (mm Hg)	40.4 ± 3.3	39.1 ± 4.0	39.3 ± 1.7	39.7 ± 3.3
MAP (mm Hg)	79.6 ± 9.0	77.1 ± 7.8	72.5 ± 0.2	77.6 ± 7.8
Temperature (°C)	38.9 ± 0.4	38.9 ± 0.5	38.4 ± 0.8	38.8 ± 0.5
Hematocrit	35.9 ± 1.1	34.1 ± 1.3	33.3 ± 1.8	34.8 ± 1.6
Dynamic CT parameters				
rCBV (mL/100 g)	2.14 ± 0.82	1.89 ± 0.69	1.42 ± 0.19	1.93 ± 0.74
rMTT (sec)	1.88 ± 1.20	1.72 ± 0.92	1.85 ± 0.86	1.81 ± 1.02
rCBF (mL/min per 100 g)	77.1 ± 30.1	76.8 ± 34.4	53.5 ± 24.3	73.3 ± 31.5
Microsphere parameters				
rCBF (mL/min per 100 g)	76.1 ± 33.4	80.3 ± 33.5	54.0 ± 4.8	74.3 ± 31.6

Note.—Values are mean ± SD; n is the number of regional measurements; three regional measurements were made per study.

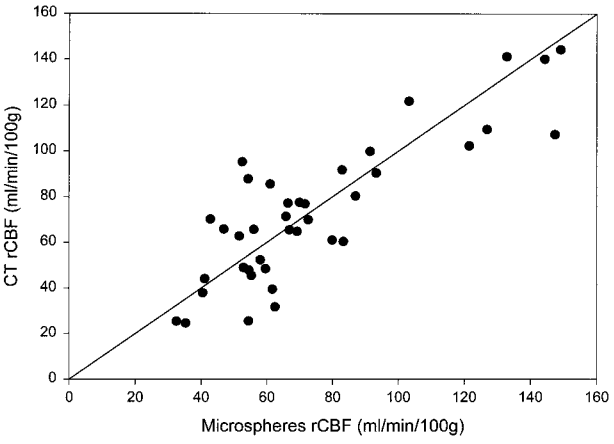

FIG 6. Dynamic CT measurements plotted against microsphere measurements of rCBF (mL/min per 100 g) for 39 ROIs. A strong correlation was found between these two sets of measurements ($r = .837$, $P < .001$). The slope of the regression line (0.97 ± 0.03) was close to unity.

namic CT and the microsphere methods are listed in Table 1. A comparison of the dynamic CT rCBF values with those determined using the standard of reference (microsphere) method revealed a significant correlation ($r = .837$, $P < .001$) between the two methods (Fig 6). The accuracy of the dynamic CT method for measuring rCBF compared well with the microsphere method, as shown by the near-unity regression slope of Figure 6 (slope = 0.97 ± 0.03).

Table 2 compares the reproducibility of the microsphere method and the dynamic CT method in measuring rCBF under steady-state conditions. The variability for each method was determined by comparing rCBF in identical ROIs from the repeated studies using ANOVA. The variability was approximately 10% higher for the CT rCBF values as compared with the microsphere data (Table 2). The differences in the CT measurements in the repeated studies, however, did not reach statistical significance ($P > .10$). The variability for the CT

TABLE 2: Comparison of the reproducibility of dynamic CT with microsphere rCBF measurements in repeated studies (n = 15) and in hemispheric (right and left) measurements) (n = 13)

Method and Hemodynamic Parameter	Variability for Repeated Measurements (%)	Right-Left Hemisphere Percentage of Difference (%)
Microsphere rCBF (mL/min per 100 g)	23.5	3.2*
CT rCBF (mL/min per 100 g)	32.5	1.9*
CT rCBV (mL/100 g)	15.5	8.4*

Note.—The percentage of variability was determined using an ANOVA for repeated measurements. Percentage of difference was calculated as $100 \times [2 \times (\text{right} - \text{left})]/(\text{right} + \text{left})$.

* Denotes no statistically significant difference ($P > .10$) as determined by *t*-test, or Mann-Whitney rank sum test.

rCBV values was better at 15.5% (Table 2), and again there was no statistically significant difference in the repeated measurements ($P >$. 10).

The side-to-side comparison of the hemispheric rCBV and rCBF values revealed only minor differences (Table 2). A *t*-test analysis revealed no significant difference in the dynamic CT or in the microsphere measurements between contralateral hemispheres ($P >$. 10).

Discussion

CT Partial Volume Averaging Correction

In CT, PVA results from the limited spatial resolution of the scanner and decreases with increased spatial resolution. Since the spatial resolution of the CT scanner used in these studies was 10 lp/cm, PVA remained an inherent source of error when imaging small blood vessels. As stated by Axel (18), because of PVA, the enhancement in small blood vessels cannot be accurately measured with CT, since their volume is averaged together with that of surrounding tissue. Owing to the much lower attenuation coefficient of the extravascular tissue, the mean CT number, reflecting the contrast concentration, within the arterial ROI will be considerably underestimated. Hence, a falsely lower arterial enhancement curve would be measured, which would result in overestimation of rCBV and of rCBF.

In our study, we demonstrated that the SD of the gaussian curve that fits the background-subtracted image profile of an artery imaged in cross section (Fig 4B) is linearly related to the diameter of the artery (Equation 7). Also, for each diameter, a PVSF can be determined to correct for the effect of PVA in the measurement of contrast enhancement (Equation 8). In the dynamic CT studies, PVSFs for the rabbit ear arteries had a mean of 1.7. Thus, without PVA correction, the arterial enhancement curve would have been underestimated, on the average, by approximately 60%, resulting in a similar overestimation of the CT rCBV and rCBF values, respectively. Our phantom studies show that when imaging an artery with an internal diameter greater than 1.73 mm (or gaussian SD > 3.2), the effect of PVA in the measurement of contrast enhancement is negligible.

However, limitations of this method must be recognized. First, it only provides an approximate correction for the PVA effect, allowing the resulting measurement error to be reduced without completely eliminating it. Second, in our rabbit studies, we selected only those arteries for PVA correction that appeared to be approximately at right angles to the scan plane. In cases in which the artery is at an oblique angle to the CT scan plane, a higher gaussian SD could be expected, resulting in the use of an inappropriate PVA correction factor. This would lead to slightly higher rCBV and rCBF measurements. Thus, we recommend applying our method only to those vessels that appear as symmetric circles on the CT scan. Finally, our method is limited to a minimum inner diameter. From the PVA phantom experiments, PE-20 tubing (0.38-mm inner diameter) did not provide any significant contrast enhancement above background. From this observation, our method cannot be used for inner diameters of less than 0.4 mm. However, our method provided accurate measurements for the smallest PE tube of the PVA phantom (ie, PE-60, 0.76-mm inner diameter).

In summary, we developed a convenient method to correct for PVA when imaging small arteries. In contrast to the work of Lapin et al (23), our method does not require any intravenous blood sampling, poststudy scans of these blood samples, or CT scans of the subject 10 minutes after contrast infusion. Our convenient method has the potential to overcome the problem of PVA in various clinical and experimental settings in which accurate measurements of intravascular contrast concentration are needed.

Dynamic CT Measurements of Cerebral Hemodynamics

The second part of this study was aimed at validating our dynamic CT rCBF measurements using a well-established technique (ie, microspheres) in a healthy animal model. To the best of our knowledge, this is the first experimental study to validate a deconvolution-based approach in the CT measurement of rCBF since the original description by Axel nearly two decades ago (21).

A strong correlation was found between the dynamic CT and the fluorescent microsphere rCBF measurements ($r =$. 835, $P < .001$). This correlation compares well with the findings of others who have validated their dynamic CT (14) and stable xenon-CT (29) techniques with microsphere measurements. Using the center of gravity of the dynamic contrast-enhancement curves to obtain rMTT values for rCBF measurements in dogs,

Gobbel et al (14) showed a strong correlation ($r = .95$) in the hemisphere and basal ganglia ROIs, but a poor correlation in the internal capsule ($r = .51$). With regard to the stable xenon-CT method, Dewitt et al (29) reported a correlation of 0.69 in seven baboons under conditions of normocapnia and 0.83 in five baboons for both hypocapnia and hypercapnia (20 and 60 mm Hg, respectively). Our mean rCBF values are similar to those obtained by other investigators in rabbits under isoflurane anesthesia (30, 31). Our results further indicate that rCBF can be measured in ROIs as small as 0.38 cm^2 in rabbits using 80 mAs per CT scan at 80 kVp for 60 scans and a contrast dose of 1.5 mL of Isovue 300 per kilogram of body weight.

The short-term reproducibility of our rCBV and rCBF measurements was approximately 15% and 30%, respectively (Table 2). The good rCBV precision (Table 2) is similar to that obtained by others, who reported variabilities of 14% in rabbits (15) and 20% in humans (22). In contrast, the precision of our CT rCBF method was lower. The fact that the variability of the microsphere results was also approximately 25% suggests that this could, in part, reflect true physiological changes due to the 30-minute delay between repeated studies. However, a similarly low rCBF precision was found by Gobbel et al (14) in repeated canine studies using only 10-minute intervals. Thus, part of this variability in our CT rCBF measurements is presumably due to methodological issues. Such low precision may have resulted from the inaccuracy of the rMTT calculations due to the inherent noise sensitivity of deconvolution (19–21). In particular, the deconvolution of noisy tissue and arterial enhancement curves may produce impulse residue functions not characteristic of the capillary bed, resulting in considerable rMTT errors. Since enhancement is linearly related to the amount of intravascular iodine (32), a better signal-to-noise ratio can be obtained by either increasing the iodine concentration in the contrast material ($>$ 300 mg I/mL) or increasing the infusion rate (0.3 mL/s in our studies) of the contrast material.

Nevertheless, an advantage of our deconvolution method is that it allows for rMTT calculations without curve-fitting or other modifications to the originally measured enhancement curves. Since the first and subsequent passage of the bolus are inherent in the arterial as well as the tissue-enhancement curves, the simultaneous imaging of an artery in the same tissue plane excludes recirculation as a potential source of error in the calculation of rMTT. Furthermore, ROI-specific MTT values can be calculated using our approach, as opposed to global values used by other investigators (15). This is of particular importance in pathologic conditions (eg, stroke) in which different and inhomogeneous rMTT values could exist between normal and ischemic regions.

The radiation dose associated with our dynamic CT method must also be considered. Although the number of images required for a dynamic CT study is about three times greater than that for a conventional head scanning protocol (60 vs 17 scans), much lower X-ray tube parameters are used (80 kVp and 80 mA vs 120 kVp and 340 mA) (33). Thus, the same effective dose equivalent of approximately 1.5 mSv (33) is delivered with our dynamic CT protocol. However, the effective dose equivalent of other blood-flow measurement techniques, such as PET and SPECT, is more than double this value (34, 35). At present, our technique is limited to a single section within the brain. In stroke patients, it is uncertain whether this single-section approach is sufficient for diagnostic purposes. It is further unclear which section has to be used to obtain useful prognostic information. The introduction of multisection CT scanners in the future may overcome this limitation. However, the increased radiation risk due to the higher dose of multisection studies must be weighed against the additional clinical benefit. Moreover, the subject may move during the dynamic CT scanning interval. Although the scanning time of 60 seconds in our dynamic CT study is much shorter than that of xenon-CT, PET, and SPECT studies, movement artifacts (especially in the *z*-direction) remain an important problem that affects the accuracy of our hemodynamic measurements. Thus, the feasibility of our technique for critically ill patients, who are unable to remain still, has yet to be evaluated.

Finally, we validated our CT rCBF method for a wide physiological range between 30 and 150 mL/min per 100 g (Fig 6). For rCBF less than 30 mL/min per 100 g, as found in ischemic tissue, the accuracy and reproducibility still have to be determined. The possible breakdown of our deconvolution method under ischemic conditions needs to be evaluated. In our deconvolution method, the algorithm will determine the optimal separation (in the least-squares sense) between the arterial and tissue-enhancement curves. Thus, any time delay between the two curves is accounted for in our method and does not lead to error in any calculation of the impulse residue function. The question of dispersion between an artery (eg, internal carotid or an ear artery) and a brain tissue region needs more attention. Our group (36) as well as other investigators (37) have shown that dispersion is not a major concern along large arteries. For the core of an ischemic region, it is reasonable to expect that the arterial input to this type of region will be subject to more dispersion than regions with normal or a slight decrease in blood flow, owing to the increase in length of the collateral pathways supplying that region. In fact, Ostergaard et al (37) have shown preliminary evidence of this phenomenon in a stroke patient. If we assume that the additional dispersion can be characterized by the function h(t), then instead of the impulse residue function, R(t), our deconvolution algorithm will calculate the convolution of h(t) and R(t); that is, h(t)*R(t). It can be shown that if the width of h(t), characterized by

the full-width-tenth-maximum, is equal to or less than the plateau width of R(t), then the maximum height of R(t), and hence the blood flow, is not affected. In addition, since the area of both R(t) and h(t)*R(t) will be the same and MTT is equal to the maximum height divided by the area of R(t), then MTT will not be affected either. If the condition of insignificant dispersion—that is, the width of h(t) is less than the plateau width of R(t)—is invalid, then the maximum height of h(t)*R(t) will underestimate the true height of R(t), hence the true blood flow. Even in this situation, the area of h(t)*R(t) will be the same as R(t), so that the calculated CBV will be correct. However, MTT will be overestimated, because blood flow is underestimated. The magnitudes of the underestimation in blood flow and overestimation of MTT cannot be quantified without detailed knowledge of h(t). In the brain, Greitz (38) has shown that the condition of insignificant dispersion is generally true both in healthy persons and in patients with compromised input pathways. This was an old study using serial (film) angiography with limited time resolution. Owing to the central importance of this assumption, it is important to repeat Greitz's results using modern DSA equipment, which is capable of much higher framing rates.

Conclusion

We have validated a new and convenient dynamic CT method to measure rCBF. The widespread availability of CT scanners, coupled with their low operating costs and the high temporal and spatial resolution of CT scans, suggests that our method can serve as an alternative diagnostic tool to assess the cerebral hemodynamics in various experimental and clinical situations.

Acknowledgments

We are grateful to animal care technologists Sarah Henderson and Monique Labodie for their surgical preparation of the rabbits and their help in obtaining the microsphere CBF measurements. The help of Laura Poczok-Stevens in the PVA phantom experiments is also acknowledged. We thank Jay Davis for his development of the Xstatpak program that was used extensively in the analysis of CT scans.

References

1. **Heart and Stroke Facts: 1994 Statistical Supplement.** Dallas: American Heart Association; 1993
2. Adams HP, Brott TG, Furlan AJ, et al. **Guidelines for thrombolytic therapy for acute stroke: a supplement to the guidelines for the management of patients with acute ischemic stroke.** *Stroke* 1996;27:1711–1718
3. Furlan A, Kanoti G. **When is thrombolysis justified in patients with acute ischemic stroke? A bioethical perspective.** *Stroke* 1997;11:214–218
4. The NINDS t-PA Stroke Study Group. **Generalized efficacy of t-PA for acute stroke: subgroup analysis of the NINDS t-PA stroke trial.** *Stroke* 1997;28:2119–2125
5. Goldman H. **Techniques for measuring cerebral blood flow.** In: Phillis JW, ed. The Regulation of Cerebral Blood Flow. Boca Raton, FL: CRC Press; 1993
6. Tyrrell P. **Tomographic measurement of cerebral blood flow and metabolism with positron emitting isotopes in man.** In: Harper AM, Jennett S, eds. Cerebral Blood Flow and Metabolism. Manchester: Manchester University Press; 1990;90–107
7. Alexandrov AV, Black SE, Ehrlich LE, et al. **Simple visual analysis of brain perfusion on HMPAO SPECT predicts early outcome in acute stroke.** *Stroke* 1996;27:1537–1542
8. Rosen BR, Belliveau JW, Chien D. **Perfusion imaging by nuclear magnetic resonance.** *Magn Reson Q* 1989;5:263–281
9. Kucharczyk J, Roberts T, Moseley ME, Watson A. **Contrast-enhanced perfusion-sensitive MR imaging in the diagnosis of cerebrovascular disorders.** *J Magn Reson Imaging* 1993;3:241–245
10. Knight R, Dereski M, Helpern J, Ordidge R, Chopp M. **Magnetic resonance imaging assessment of evolving focal cerebral ischemia.** *Stroke* 1994;25:1252–1262
11. Berninger WH, Axel L, Norman D, Napel S, Redington RW. **Functional imaging of the brain using computed tomography.** *Radiology* 1981;711–716
12. Nagata K, Asano T. **Functional image of dynamic computed tomography for the evaluation of cerebral hemodynamics.** *Stroke* 1990;21:882–889
13. Lo EH, Rogowska J, Batchelder KF, Wolf GL. **Hemodynamical alterations in focal cerebral ischemia: temporal correlation analysis for functional imaging.** *Neurol Res* 1996;18:150–156
14. Gobbel GT, Cann CE, Iwamoto HS, Fike JR. **Measurement of regional cerebral blood flow in the dog using ultrafast computed tomography: experimental validation.** *Stroke* 1991;22: 772–779
15. Hamberg LM, Hunter GJ, Halpern EF, Hoop B, Gazelle GS, Wolf GL. **Quantitative high-resolution measurement of cerebrovascular physiology with slip-ring CT.** *AJNR Am J Neuroradiol* 1996;17:639–650
16. Axel L. **A method for calculating brain blood flow with a CT dynamic scanner.** *Adv Neurol* 1981;30:67–71
17. Yonas H. **Cerebral Blood Flow Measurement with Stable Xenon-Enhanced Computed Tomography.** New York: Raven Press; 1992
18. Axel L. **Cerebral blood flow determination by rapid-sequence computed tomography: a theoretical analysis.** *Radiology* 1980; 137:679–686
19. Gamel J, Rousseau WF, Katholi CR, Mesel E. **Pitfalls in digital computation of the impulse response of vascular beds from indicator dilution curves.** *Circ Res* 1973;32:516–523
20. Bronikowski TA, Dawson CA, Linehan JH. **Model-free deconvolution techniques for estimating vascular transport functions.** *Int J Biomed Comput* 1983;14:411–429
21. Axel L. **Tissue mean transit time from dynamic computed tomography by a simple deconvolution technique.** *Invest Radiol* 1983;18:94–99
22. Steiger HJ, Aaslid R, Stooss R. **Dynamic computed tomography imaging of regional cerebral blood flow and blood volume: a clinical pilot study.** *Stroke* 1993;24:591–597
23. Lapin GD, Munson RJ, Groothius DR. **Noninvasive CT determination of arterial blood concentration of meglumine iothalamate.** *J Comput Assist Tomogr* 1993;17:108–114
24. Meier P, Zierler KL. **On the theory of the indicator-dilution method for measurement of blood flow and volume.** *J Appl Physiol* 1954;6:731–744
25. Roberts GW, Larson KB. **The interpretation of mean transit time measurements for multi-phase tissue systems.** *J Theor Biol* 1973;39:447–475
26. Bassingthwaighte JB, Chinard FP, Crone C, Lassen NA, Perl W. **Definitions and terminology for indicator dilution methods.** In: Crone C, Lassen NA, eds. Capillary Permeability. Copenhagen: Munskgaard; 1970
27. Yeung IWT, Lee T-Y, Del Maestro RF, Kozak R, Bennet JB, Brown T. **An absorptiometry method for the determination of arterial blood concentration of injected iodinated contrast agent.** *Phys Med Biol* 1992;37:1741–1758
28. Heymann MA, Payne BD, Hoffman JI, Rudolph AM. **Blood flow measurements with radionuclide-labeled particles.** *Prog Cardiovasc Dis* 1977;20:55–79
29. Dewitt DS, Fatouros PP, Wist AO, et al. **Stable xenon versus radiolabeled microsphere cerebral blood flow measurements in baboons.** *Stroke* 1989;20:1716–1723
30. Todd MM, Wu B, Warner DS, Maktabi M. **The dose-related effects of nitric oxide synthase inhibition on cerebral blood flow during isoflurane and pentobarbital anesthesia.** *Anesthesiology* 1994;80:1128–1136

31. Patel PM, Mutch WAC. **The cerebral pressure-flow relationship during 1.0 MAC isoflurane anesthesia in the rabbit: the effect of different vasopressors.** *Anesthesiology* 1990;72:118–124
32. Fike JR, Cann CE, Berninger WH. **Quantitative evaluation of the canine brain using computed tomography.** *J Comput Assist Tomogr* 1982;6:325–333
33. Atherton JV, Huda W. **Energy imparted and effective doses in computed tomography.** *Med Phys* 1996;23:735–741
34. Huda W, Sandison GA. **Estimates of the effective dose equivalent, H_E, in positron emission tomography studies.** *Eur J Nucl Med* 1990;17:116–120
35. Huda W, Sandison GA. **The use of the effective dose equivalents, H_E, for 99mTc labelled radiopharmaceuticals.** *Eur J Nucl Med* 1989;15:174–179
36. St Lawrence KS, Lee T-Y. **An adiabatic approximation to the tissue homogeneity model for water exchange in the brain, II: experimental validation.** *J Cereb Blood Metab* (in press)
37. Ostergaard L, Sorensen AG, Kwong KK, Weisskoff RM, Gyldensted C, Rosen BR. **High resolution measurement of cerebral blood flow using intravascular tracer bolus passages, II: experimental comparison and preliminary results.** *Magn Reson Med* 1996;36:726–736
38. Greitz T. **A radiologic study of the brain circulation by rapid serial angiography of the carotid artery.** *Acta Radiol Suppl* 1956;140:1–123